Missouri University of Science and Technology
Scholars' Mine

Materials Science and Engineering Faculty Research & Creative Works

Materials Science and Engineering

15 Jun 2020

Resistive switching in atomic layer deposited HfO2/ZrO2 nanolayer stacks

Lin Tang

Hiraku Maruyama

Taihao Han
Missouri University of Science and Technology, thy3b@mst.edu

Juan C. Nino

et. al. For a complete list of authors, see https://scholarsmine.mst.edu/matsci_eng_facwork/3263

Follow this and additional works at: https://scholarsmine.mst.edu/matsci_eng_facwork

Part of the Materials Science and Engineering Commons

Recommended Citation

L. Tang et al., "Resistive switching in atomic layer deposited HfO2/ZrO2 nanolayer stacks," *Applied Surface Science*, vol. 515, article no. 146015, Elsevier, Jun 2020.
The definitive version is available at https://doi.org/10.1016/j.apsusc.2020.146015

This Article - Journal is brought to you for free and open access by Scholars' Mine. It has been accepted for inclusion in Materials Science and Engineering Faculty Research & Creative Works by an authorized administrator of Scholars' Mine. This work is protected by U. S. Copyright Law. Unauthorized use including reproduction for redistribution requires the permission of the copyright holder. For more information, please contact scholarsmine@mst.edu.

Applied Surface Science 515 (2020) 146015

Contents lists available at ScienceDirect

Applied Surface Science

journal homepage: www.elsevier.com/locate/apsusc

Full Length Article

Resistive switching in atomic layer deposited HfO_2/ZrO_2 nanolayer stacks

Lin Tang[a], Hiraku Maruyama[b], Taihao Han[b], Juan C. Nino[b,*], Yonghong Chen[a], Dou Zhang[a,*]

[a] *State Key Laboratory of Powder Metallurgy, Central South University, Changsha 410083, China*

[b] *Department of Materials Science and Engineering, University of Florida, Gainesville, FL 32611, United States*

ARTICLE INFO

Keywords:
Resistive switching
HfO_2/ZrO_2
Nanolayer
Interfaces

ABSTRACT

The resistive switching properties of HfO_2/ZrO_2 nanolayers with the total thickness of 16 nm prepared using atomic layer deposition (ALD) were investigated. Current-voltage behavior, pulse time mode measurement, retention and endurance tests were carried out to characterize the memristive (memory-resistive) properties. Resistive switching was observed in all nanolayer stacks, and the set voltage (V_{set}) decreased with increasing the number of layers (i.e., increasing number of hafnia-zirconia interfaces). Grazing incidence x-ray diffraction (GI-XRD) results demonstrate that the hafnia transforms from monoclinic to orthorhombic crystal structure during the post metallization annealing. Shifts in the binding energy of the x-ray photoelectron spectra (XPS) implies the existence of hafnia and zirconia suboxide ($HfO_{2\text{-}\delta}$ and $ZrO_{2\text{-}\delta}$). Moreover, the blocking nature of the inserted oxide/oxide interfaces serves as a barrier to oxygen ion/vacancy migration. It is shown that memristive/insulating nanostructures like HfO_2/ZrO_2 can help modulate the resistive switching of memristor-based devices.

1. Introduction

In the past decade, non-volatile memory devices, such as ferroelectric random access memory (FRAM), ferroelectric filed effect transistor (FE-FET), ferroelectric tunneling junction (FTJ), energy storage device as well as resistive random access memory (RRAM), have been paid much attention for next-generation memory applications [1–7]. RRAM which utilizes reversible resistive switching to recognize the “0″ or “1” in logic circuits for data storage is based on a Metal-Insulator-Metal (MIM) structure, and thus, usually requires a dielectric material as insulating layer [8]. Compared with traditional lead-based perovskite materials used in FRAM like lead zirconate titanate (PZT), simple binary HfO_2 and ZrO_2 are environmentally friendly and easily integrated into complementary metal–oxidesemiconductor (CMOS) technology [9]. Moreover, given the recent developments in advanced deposition techniques, HfO_2 and ZrO_2 are suitable for three-dimensional (3D) integration of capacitors and thereupon are promising candidates for resistive switching layers in RRAM structures [10]. Li et al. reported the resistive properties of $Au/ZrO_2/Ag$ structures under low operation voltages (< 1 V) and fast switching speed (50 ns) [11]. Since the ferroelectricity was reported in Si doped HfO_2 thin films in 2011, there have been numerous efforts focused on the resistive switching properties of HfO_2-based ferroelectric thin films [12–15]. Recently, Yoong et al [7] reported an extremely large ferroelectric resistive switching with a R_{OFF}/R_{ON} ratio of 16100% in epitaxial ferroelectric $Hf_{0.5}Zr_{0.5}O_2$ (HZO) resistive memory devices. Furthermore, a redox-type reaction of the TiN layer at the interface with the HfO_2 film is believed as the possible origin of the bipolar switching, which was further introduced and developed in the bilayer structure of HfO_2/ZrO_2 films [16]. Considering that multilayer structures have been identified as a feasible route to increase interfaces and regulate the migration of oxygen ions and vacancies [17], in this work, we investigated the resistive switching of HfO_2/ZrO_2 nanolayer structures for modulating the conductive filaments.

2. Experimental section

HfO_2/ZrO_2 multilayer stacks with a total thickness of 16 nm were deposited on $Pt/Ti/SiO_2/Si$ substrates using ALD method. Tetrakis (ethylmethylamino)-hafnium (TEMAH, Fornano, 99.999%), tetrakis (ethylmethylamino)-zirconium (TEMAZ, Fornano, 99.999%) and ultrapure H_2O were used as Hf precursor, Zr precursor and oxidant, respectively. The substrates were cleaned under ultrasonic agitation in acetone, ethanol, and deionized water for 10 min, and then dried with a nitrogen gun. To obtain the nanolayer films, HfO_2 and ZrO_2 layers with different thickness were alternatively deposited at 250 °C, as shown in Fig. 1(a). By tuning the number of pulse cycles during deposition, four types of structures were prepared, such as N1 ((8 nm HfO_2 + 8 nm ZrO_2) × 1), N2 ((4 nm HfO_2 + 4 nm ZrO_2) × 2), N4 ((2 nm HfO_2 + 2 nm ZrO_2) × 4) and N8 ((1 nm HfO_2 + 1 nm ZrO_2) × 8). A

* Corresponding authors.
E-mail addresses: jnino@mse.ufl.edu (J.C. Nino), dzhang@csu.edu.cn (D. Zhang).

https://doi.org/10.1016/j.apsusc.2020.146015
Received 13 November 2019; Received in revised form 29 February 2020; Accepted 7 March 2020
Available online 10 March 2020
0169-4332/ © 2020 Elsevier B.V. All rights reserved.

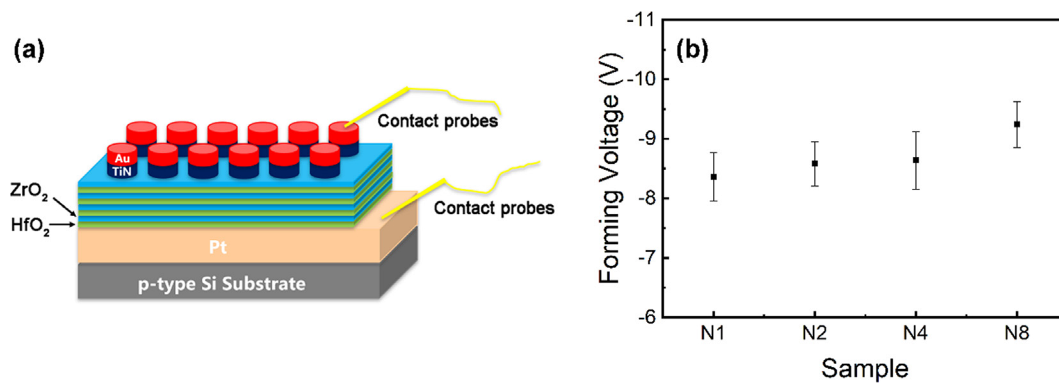

Fig. 1. (a) Schematic structure of the nanolayered films. HfO_2/ZrO_2 films are stacked alternatively on the $Pt/Ti/SiO_2/Si$ substrates to form the nanolayer structure. (b) Average forming voltage of four types of samples.

capping layer of TiN (30 nm thick) and Au top electrode (100 nm thick) were deposited using DC magnetic sputtering covered with a metal shadow mask (300 µm diameter). The obtained MIM structures were annealed under 450 °C in nitrogen atmosphere for 30 s using rapid thermal processing (RTP). Grazing incidence x-ray diffraction (GI-XRD, Bruker D8 Advanced, Cu-Kα radiation, λ = 0.154 nm) was used to determine the crystal structure of the HfO_2/ZrO_2 nanolayers with a grazing incident angle of 0.5°. X-ray photoelectron spectroscopy (XPS, ESCALAB250Xi, Thermo) analysis was performed to observe the bonding structure and valences of the chemical species. The electrical characterization was performed using a semiconductor parameter analyzer (Agilent 4156C) at room temperature and included current-voltage (*I-V*), pulse mode test, retention, and endurance reliability measurement. During the test, the left probe was contacted with the top electrode and the right probe was grounded. Moreover, 4–6 cells were measured on each sample and a compliance current (CC) of 10^{-4} A was used to prevent the samples from electrical breakdown.

3. Results and discussion

Fig. 2 shows the semi log current-voltage behavior of Au/TiN/$(ZrO_2/HfO_2)_n$/Pt devices. For each sample, a voltage sweep applied on the top electrode (1 → 2 → 3 → 4 shown in the figures) was followed and the resistive switching behavior was observed. It is important to note that a large negative voltage was needed to electroform the first conductive state in the device in order to activate the reversible resistive switching behavior [18]. Forming current fluctuations were observed with increasing voltage, as shown in the right insets of Fig. 2(a)–(d). Since the average forming voltage of these four samples increased from −8.4 V to −9.2 V (Fig. 1(b)), it can be inferred that this is the result of voltage drop at the additional zirconia-hafnia interfaces. After the forming process, all the samples showed an initial HRS and underwent the resistive switching from HRS to LRS in the first cycle, which was consistent with the formation of conductive filaments in these oxide layers. To investigate the conducting mechanism of HRS, the $\text{Ln}(I) - V^{1/2}$ curve fitting method [19] was used. In the left insets of Fig. 2(a)-(d), a linear relationship in these fits was observed, which was indicative of a Schottky emission mechanism active in the HRS at low voltages ($|V| < 1$ V). In addition, the set process of each sample was investigated. Although the abrupt increase in current was not immediately observed in N1 samples from 0 to −3 V, the current showed a gradually continuous increase during the set process and a gradual LRS-to-HRS transition during the reset process (Fig. 2(a)). In Fig. 2(b), the N2 devices exhibited a typical bipolar resistive switching with the set voltage (V_{set}) of −1.5 V and the reset voltage (V_{reset}) of approximately +1.5 V. However, the N4 samples exhibited an interesting resistive switching behavior. It is worth noting that at the first cycle, after the first abrupt increase in current, there was a plateau in the N4 sample until the current suddenly increased again and reached the CC level as shown in Fig. 2(c). The V_{set} of N2 samples was larger than the V_{set1} (−1.25 V) and smaller than the V_{set2} (−1.8 V) of N4. Such lower V_{set1} can be attributed to the formation of conductive filaments in the first HfO_2/ZrO_2 interfaces near the TiN [20]. Therefore, it can be inferred that the emergence of a potential barrier at the interfaces between the alternatively deposited HfO_2/ZrO_2 layers prohibits the drift of oxygen ions/vacancies, resulting in the increase of the V_{set2} in N4. In N8 samples, the V_{set1} (−1.1 V) was smaller than that of N4 (−1.25 V); interestingly however, there was no plateau after the first abrupt increase in current, which pointed to differences in the formation of local conductive filaments in the HfO_2/ZrO_2 interfaces.

In order to try to understand the origin of the bipolar switching characteristics observed in the nanolayer samples, Fig. 3 shows the anticipated energy band diagram for the N1 configuration. The conduction band offset is presented in Fig. 3(a). Compared with Pt electrode, electrons can jump more easily from the TiN electrode into the ZrO_2 layer and oxygen ions migrate to the bottom electrode while applying a negative voltage. Thus, a large amount of oxygen vacancies emerges and forms a conducting path in HfO_2 and ZrO_2 layers when the applied negative voltage increases to the forming voltage, leading to the transition from HRS to LRS [16]. In this situation, a large current is generated and reaches the CC value towards the Pt electrode (Fig. 3(b)). In Fig. 3(c), when applying a positive voltage, oxygen vacancies drift back to oxide layers and the conductive filament is ruptured at the HfO_2/ZrO_2 interface since it has the smaller barrier gap [11]. Therefore, the device switches from LRS to HRS.

To further investigate the resistive switching characteristics of the samples, the cyclic voltammetry was performed on N2 and N8 configuration, respectively. In Fig. 4(a), the typical shape of the *I-V* curves was stable after 10 switching cycles, indicating the stabilization of the resistive switching behavior in N2 samples. The evolution of operation voltage in N2 for the first 10 consecutive switching cycles is shown in the left inset of Fig. 4(a), and the fluctuation of the V_{set} and V_{reset} can be easily observed. In this figure, the V_{set} had a narrow distribution (between −0.8 and −1 V), whereas the V_{reset} had a wider voltage fluctuation (between 1.5 and 2.4 V). By contrast, the resistive switching characteristics of the N8 configuration was quite different. In Fig. 4(b), the semi log *I-V* curve of N8 indicated a bipolar resistive switching in the first cycle, whereas in the 6th switching cycle, the set procedure became slightly indistinct and the reset procedure had almost disappeared; in essence, the samples transitioned from bipolar resistive switching to HRS, as shown in Fig. 4(c). Finally, in Fig. 4(d), neither SET nor RESET procedure showed up in the 10th switching cycle and the *I-V* curve behaved as a gradual HRS-to-LRS or LRS-to-HRS transition. One reasonable explanation for the resistive switching degradation of N8 is the drift of the oxygen ions/vacancies at HfO_2/ZrO_2 interface. As the thickness of each HfO_2 and ZrO_2 layer decreases, the

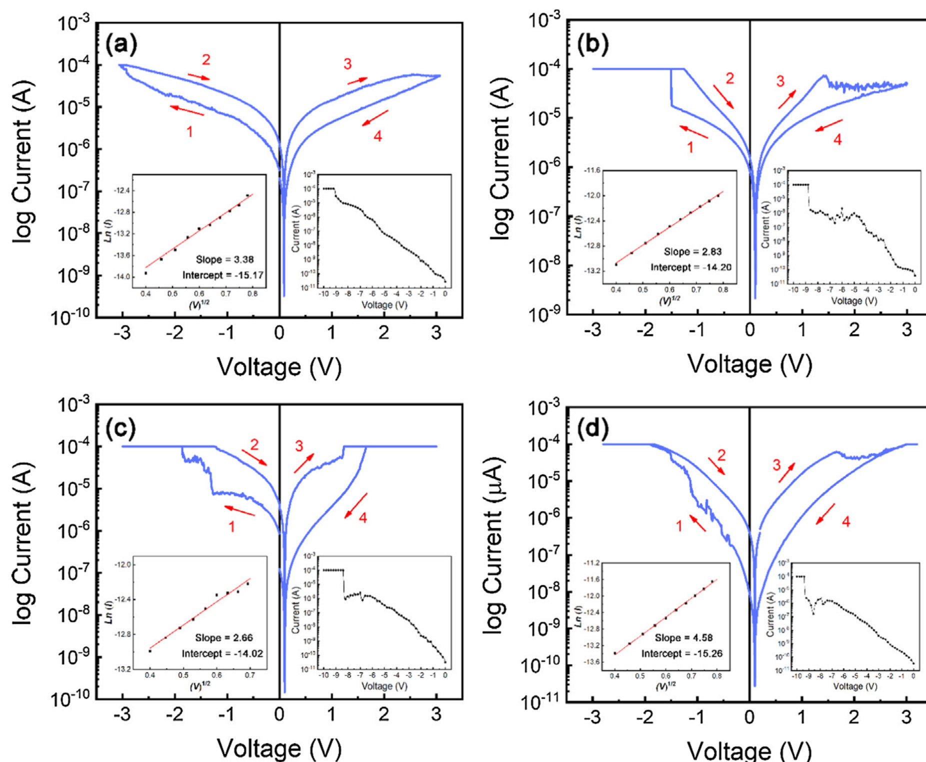

Fig. 2. Semi log I-V curves of HfO_2/ZrO_2 nanolayered films, (a) for N1, (b) for N2, (c) for N4 and (d) for N8. Both compliance currents of these four samples were set as 10^{-4} A to prevent from electrical broke down. Left and right insets show the Ln (I) – $V^{1/2}$ curve and the forming voltage, respectively.

barrier gap of the HfO_2/ZrO_2 interface is smaller due to the limited distance for oxygen ions migration. During electric field cycling, the barrier width tends to be narrower until it disappears in the end possibly because of the in-built electric field at interfaces. Therefore, the resistive switching becomes weaker and weaker with the cycles. Another reason for this behavior might be the decrease in the Schottky barrier height due to the accumulation of oxygen ions at the TiN/ZrO_2 interface [19], resulting in the electric breakdown on the TiON and the degradation of resistive switching during the electric field cycles.

Fig. 5 exhibits the real-time monitoring of 10 consecutive pulse mode measurement results of the four samples. Three read pulses after one write pulse were applied in one cycle and repeated for 10 cycles. The pulse width and pulse period were 0.1 s and 1 s, respectively. The results indicated that all the samples underwent resistive switching under an appropriate pulse condition. In Fig. 5(a), the R_{HRS}/R_{LRS} ratio of N1 remained between 2 and 3 in the initial 9 pulses and had slightly increased to ~4–5 at the end of test. In N2 samples, the R_{HRS}/R_{LRS} ratio seemed more stable with an approximate value of 7, shown in Fig. 5(b). However, the memory window of N4 and N8 had wider fluctuation. In Fig. 5(c), the R_{HRS}/R_{LRS} ratio of N4 increased from 4 to 9, whereas in Fig. 5(d), the R_{HRS}/R_{LRS} ratio of N8 suggested a dramatic decrease to 10 although it had a large R_{HRS}/R_{LRS} value of 100 at the first pulse. This degradation of the R_{HRS}/R_{LRS} ratio in N8 can be ascribed to the variation of resistive switching mechanism as mentioned in Fig. 4(b)–(d). At the beginning, the HfO_2/ZrO_2 interfaces seem to constitute the largest potential drop under the same electric field because of the existence of barrier gap between two oxide layers, causing a larger R_{HRS}/R_{LRS} ratio. However, during the measurement, the fluctuation of R_{HRS} also increased in those samples, implying that an unstable resistive switching took place under the same pulse parameters. This phenomenon is likely the result of decreased oxygen vacancy migration and the presence of charged defects at the HfO_2/ZrO_2 interface, leading to the degradation of R_{HRS} [24–26]. In this work, the N2 configuration presents a more stable switching behavior in a rapid write-read pulse operation for 10 cycles than that of N4 and N8 samples with the same level of R_{HRS}/R_{LRS} ratio in the end. In other words, the nanolayer devices with less layers or relatively larger thickness perform better in the long-time operation.

Given their superior performance, the retention characteristics of

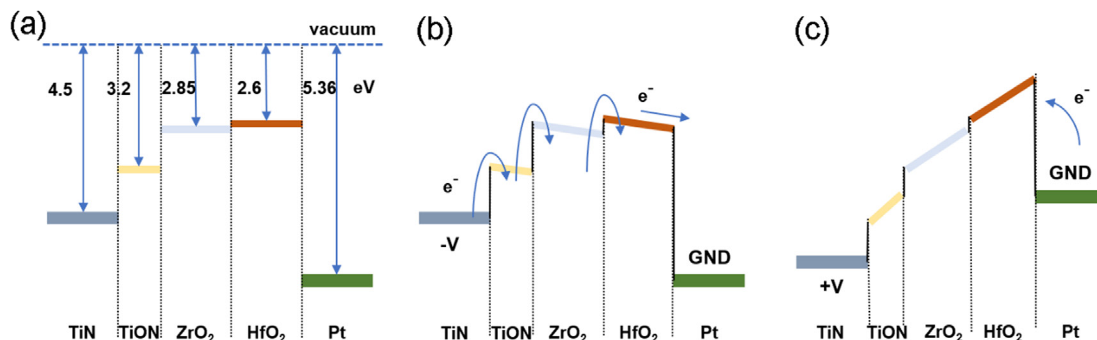

Fig. 3. The energy band diagram at (a) conduction band offset, (b) applying a negative voltage and (c) applying a positive voltage on the top electrode in N1 configuration device. The work functions of TiN (4.5 eV); the electron affinities of ZrO_2 (2.8 eV), HfO_2 (2.65 eV), and TiON (3.2 eV) are found in Refs. [21–23].

 Applied Surface Science 515 (2020) 146015

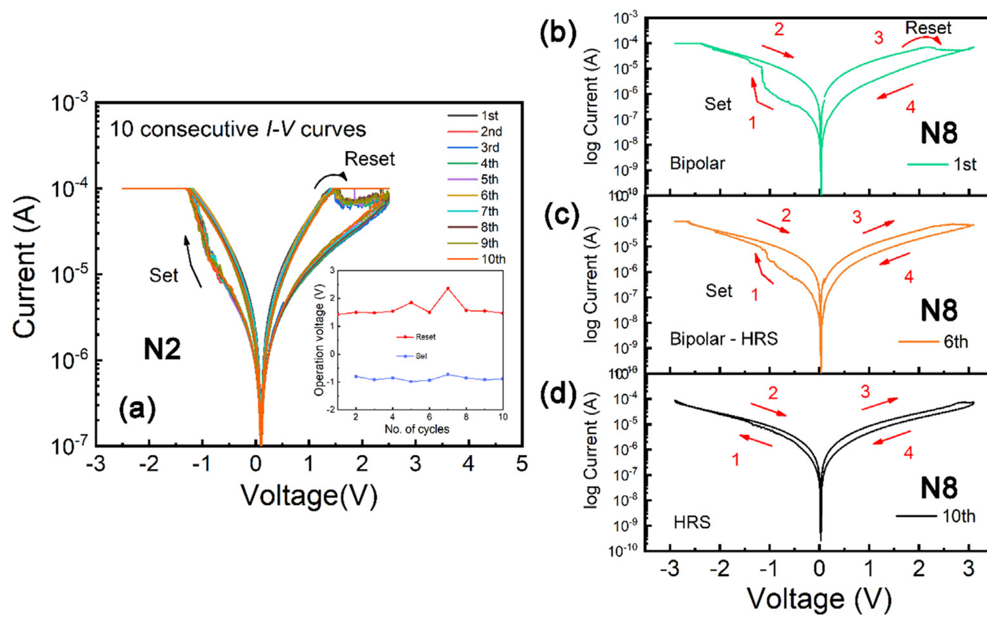

Fig. 4. (a) 10 consecutive switching cycle for N2 samples. The right insert shows the variation in operation voltage with resistance switching cycle. Semi log *I-V* curves of N8 samples in the (b) 1st, (c) 6th and (d) 10th switching cycle.

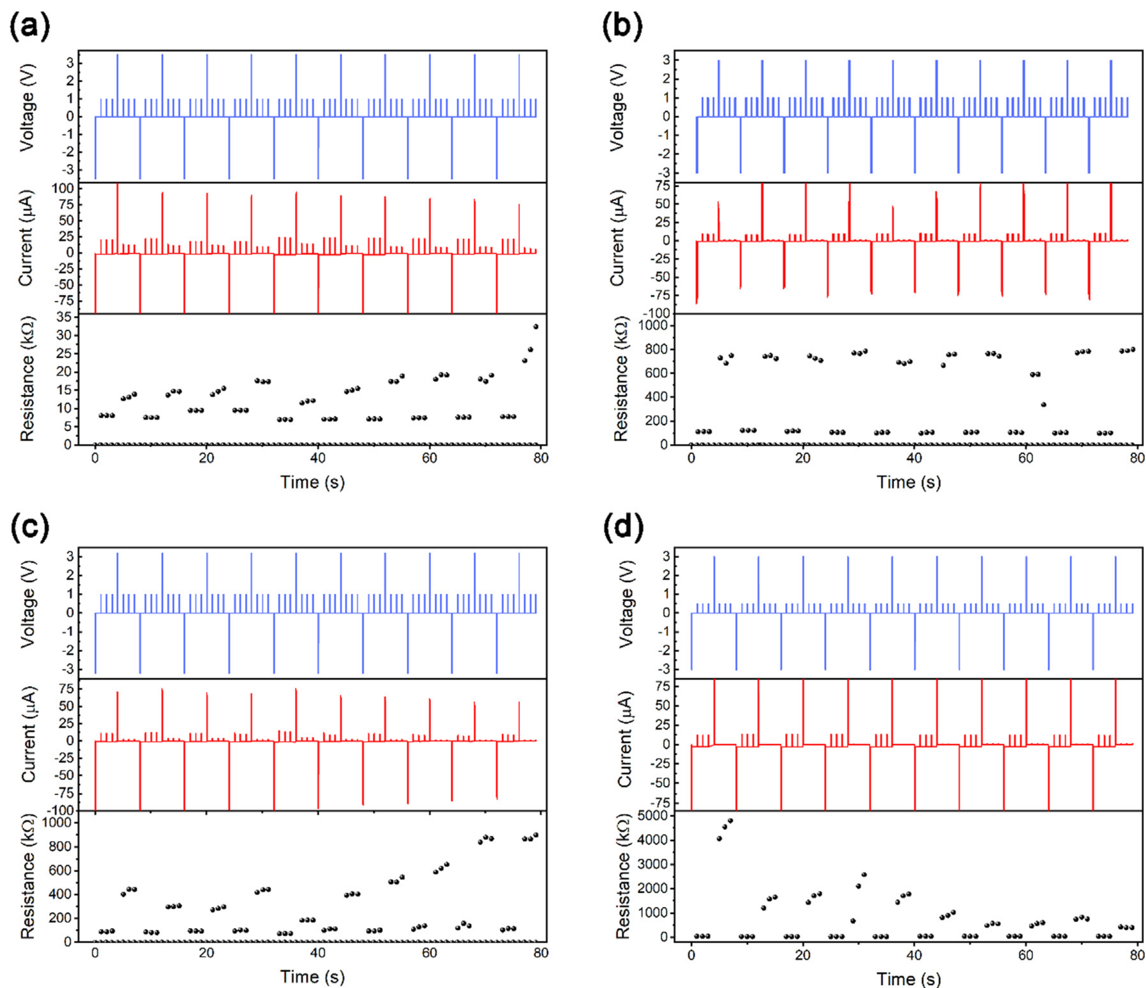

Fig. 5. Pulse mode test results of the MIM devices for (a) N1, (b) N2, (c) N4 and (d) N8.

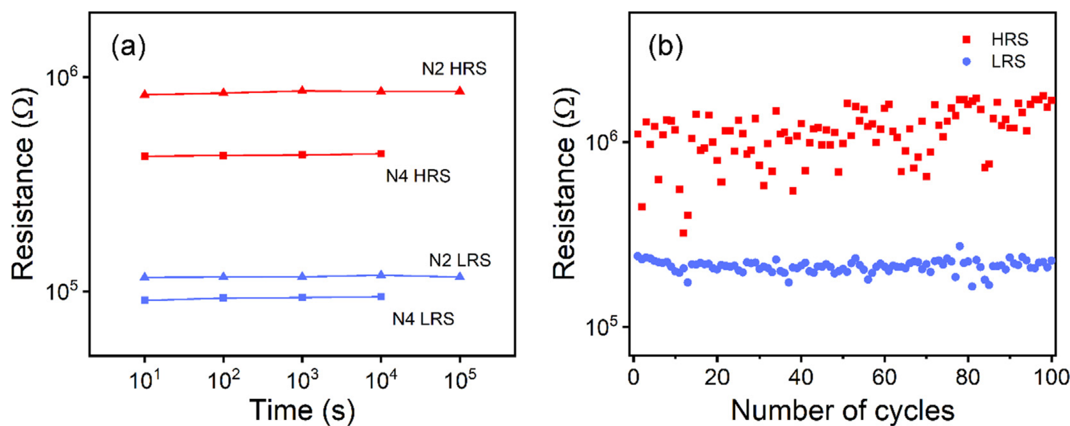

Fig. 6. (a) Retention characteristics of nanolayered device in N2 and N4 samples for at least 104 s under the write pulse amplitude as −3 V and read pulse amplitude as 0.5 V. (b) Evolution of HRS and LRS in N2 samples under electric stimuli cycles with the write pulse amplitude as −3 V and read pulse amplitude as 0.5 V.

N2 and N4 samples were also investigated. In Fig. 6(a), although the resistance of HRS slightly increased, both the R_{HRS} and R_{LRS} in N2 and N4 were respectively maintained for at least 10^5 and 10^4 s after a write operation, indicating that the HRS and LRS can be retained for a long period time without an external voltage stimulus. This result also indicates a better performance of resistive switching in N2 not only due to the larger R_{OFF}/R_{ON} ratio but also the longer retention time. To estimate the endurance capacity, the endurance test was performed on N2 samples under the write pulse amplitude of ± 3 V and read pulse amplitude of 0.5 V. In Fig. 6(b), after 100 electric field cycles, the R_{OFF}/R_{ON} ratio in N2 was stable within an order of magnitude. In nanolayer stacks, the HfO_2/ZrO_2 interface is more likely to be the place where the formation and rupture of the conductive filament takes place, rather than at the electrodes [16], and therefore the LRS can keep relatively stable during the cycles. Compared to Zr doped HfO_2 devices, it is easier to achieve the operation on the OFF/ON switching at the HfO_2/ZrO_2 interface and enhance the reliability of the devices. Both the results of retention and endurance measurements for N2 samples are promising and encouraging for further investigation into multilayer device approaches towards memrisitive device fabrication.

In order to understand the differences in the crystal structure of the samples, GI-XRD was collected on HfO_2/ZrO_2 nanolayer stacks on Pt/Ti/SiO_2/Si substrates; the representative patterns are shown in Fig. 7. The highest intensity diffraction peak observed near 45° was from Pt

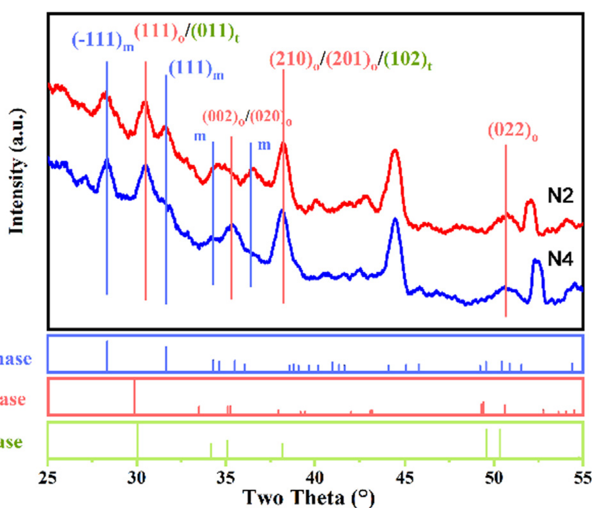

Fig. 7. GI-XRD patterns of nanolayered structures. As the thickness of monolayer decreased, monoclinic HfO_2 gradually transformed into orthorhombic HfO_2 through the surface energy and mechanical strain effects.

substrate. Both the oxidized nanolayers of N2 and N4 were polycrystalline, consisting of a combination of monoclinic, orthorhombic, and tetragonal HfO_2, as well as ZrO_2. Interestingly, as the thickness of each layer decreases, the intensity of the diffraction peak of monoclinic HfO_2 phase, labeled as $(1\ 1\ 1)_m$, significantly weakened. In addition, the $(2\ 0\ 0)_m$ at 35.5° disappeared and the $(0\ 0\ 2)_o/(0\ 2\ 0)_o$ of HfO_2 located at 35.1°/35.2° became stronger. This suggests that the metastable orthorhombic HfO_2 phase can be stabilized by the increasing interfacial energy effects as the thickness of the monolayers is reduced [27]. Due to the chemical similarity of these two fluorite structure oxides, tetragonal ZrO_2 was also stabilized for small crystallite sizes and a narrow range of surface/interface area [28]. In terms of resistive switching, it is interesting to note that while the formation energy of oxygen vacancy in tetragonal and orthorhombic HfO_2 phase was lower than that in monoclinic phase, leading to a decrease of electroforming voltage [26], the presence of HfO_2/ZrO_2 interfaces with high density of traps increased the built-in electric field by absorbing the charged defects, and thereupon increased the forming voltage [29]. Therefore, considering these two contrasting points, in this work the interfaces play a more important role on the modulation of electroforming voltage. In addition, except for the ionic migration under the applied electric field, there was a high concentration of oxygen vacancies emerging in the ZrO_2 layers near the TiN, which was ascribed to the formation of TiON interface layer during the RTP process [16]. Therefore, it can be inferred that in the case of N4, these interface barriers block the transport of the oxygen ions/vacancies, and thus, result in the high V_{set2} observed in N4.

Fig. 8 shows the XPS high-resolution spectra of Hf 4f, Zr 3d and O 1s for N2 and N4, where the C 1s peak as 284.6 eV was used for calibration. In Fig. 8(a), the Hf 4f spectrum of N2 consisted of two parts, Hf $4f_{7/2}$ at 17.1 eV and Hf $4f_{5/2}$ at 18.7 eV respectively, which was larger than the Hf $4f_{7/2}$ at 16.8 eV and Hf $4f_{5/2}$ at 18.4 eV in N4 sample [30]. This shift was consistent with a decrease in the binding energy of Hf-O bond and a high concentration of oxygen vacancies, demonstrating the formation of hafnium suboxide ($HfO_{2-\delta}$). Meanwhile, according to the standard peaks of Zr $3d_{5/2}$ at 181.7 eV [30], a similar situation occurred in the zirconium oxide layers shown in Fig. 8(b), where the Zr 3d spectrum shifted towards the higher binding energy due to the emergence of the zirconium suboxide ($ZrO_{2-\delta}$). Hence, as expected, the amount of $HfO_{2-\delta}$ and $ZrO_{2-\delta}$ in N2 was much larger than that in N4. In addition, Fig. 8(c) and (d) show the different O 1s peak spectra between the nanolayered N2 and N4 samples. The O 1s peak was deconvoluted into three parts: O_{O-Zr}, O_{O-Hf}, and $O_{non-lattice}$, which were related to the contributions of lattice oxygen and non-lattice oxygen, respectively [31]. The area proportion of each peak was also obtained in Fig. 8(c) and (d). It is worth noting that the percentage of non-lattice oxygen at 531.7 eV in N2 is 14.5%, which was larger than that of 13.2% at

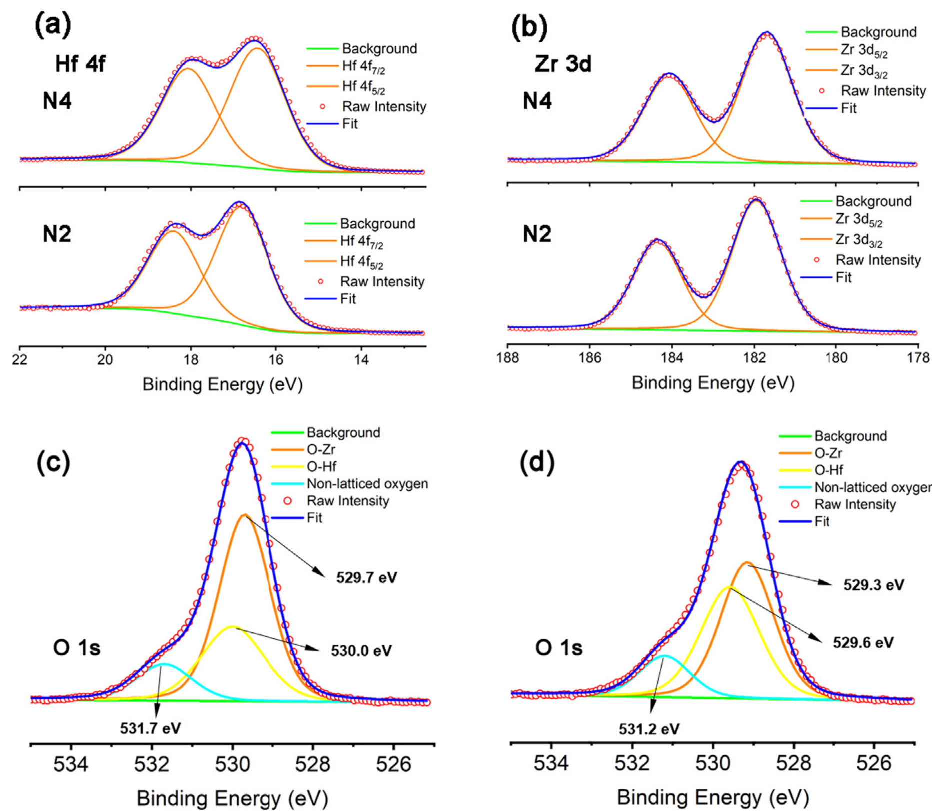

Fig. 8. XPS core level spectra of HfO_2/ZrO_2 nanolayers with deconvoluted peaks of (a) Hf 4f spectrum, (b) Zr 3d spectrum, (c) O 1s spectrum of N2 sample and (d) O 1s spectrum of N4 sample. All the spectra were calibrated by setting C 1s standard peak at 284.68 eV.

531.2 eV in N4. This difference in the oxygen distribution and location might be contributing to the lower V_{set} in N2 samples compared with N4 samples in the first cycle.

Table 1 presents a summary of switching characteristics and oxygen binding of the samples in this work. It is well known that a certain amount of oxygen vacancies is essential to complete the first electroforming step. For example, Yang et al. [18] have shown that the nature of oxide electroforming was an electro-reduction and vacancy formation process under high electric fields. Fig. 9 shows the mechanism schematic diagram of N2 configuration. According to Huang's report, after the post annealing process an extremely thin TiON layer is expected to form between TiN and ZrO_2 as a result of oxygen ion migration [16], and thus, a higher concentration of oxygen vacancies exists in both ZrO_2 and HfO_2 layers (Fig. 9(a)). When a negative bias is applied, oxygen vacancies drift and oxygen ion transfers from TiN electrode to Pt electrode, causing the resistive switching from HRS to LRS once a conductive filament emerges in the resistive switching layers (Fig. 9(b)). On the contrary, under the positive bias, the rupture of conductive filament occurs at the weakest region like HfO_2/ZrO_2 interface with smaller barrier height, leading to the resistance state switch from LRS to HRS (Fig. 9(c)). Notably, as the number of interfaces increases the more rupture region can be established, which might enhance the randomness of the rupture of the conductive filament but reduce the stability of the resistance of HRS either (Fig. 6(b)). In addition, in the N4 nanolayer devices, local conductive filaments are likely to form in the first several oxide layers through oxygen vacancy migration as shown in Fig. 2(c); the resistance state alters from HRS to a medium state and kept stable until the voltage increases to a higher value (V_{set2}). Once the applied voltage reached V_{set2}, the complete conductive filament forms throughout the nanolayer films and the resistance state switches from medium state to LRS. This not only suggests that the HfO_2/ZrO_2 interfaces further limit the migration of the oxygen ion/vacancy but explains the observed increase in V_{set} and a larger R_{OFF}/R_{ON} ratio as the number of interface increases.

4. Conclusions

In summary, HfO_2/ZrO_2 nanolayer stacks can be successfully fabricated using ALD, and their resistive switching characteristics were studied. As the number of HfO_2/ZrO_2 interface increases, HfO_2 and ZrO_2 transform from monoclinic to orthorhombic and tetragonal phase, respectively. The shifts of binding energy in XPS results demonstrates the formation of hafnia and zirconia suboxides (i.e., $HfO_{2-\delta}$, $ZrO_{2-\delta}$), meantime the decrease in the percentage of $O_{non\text{-}lattice}$ indicates the suppression of the oxygen ion/vacancy migration via introducing the HfO_2/ZrO_2 interfaces. The device with more HfO_2/ZrO_2 interfaces shows a higher R_{HRS}/R_{LRS} ratio, however, it presents a degradation of the memory windows during the cycles. This phenomenon is probably

Table 1
Summary of switching characteristics and oxygen bonding distribution.

Samples	Forming Voltage (V)	V_{set}/V_{reset}	R_{OFF}/R_{ON} Ratio	Phase	Percentage of non-lattice oxygen	Percentage of Zr-O bond	Percentage of Hf-O bond
N1	−8.4	−/−	2–3	*m*-	17.0%	69.9%	13.1%
N2	−8.7	−0.9/+1.4	7–8	*m*-, *t*-, *o*-	14.5%	57.9%	27.6%
N4	−8.6	−/−	4–9	*m*-, *t*-, *o*-	13.2%	45.8%	41.0%
N8	−9.4	−1.3/+1.8	10–100	*t*-, *o*-	12.9%	43.2%	43.9%

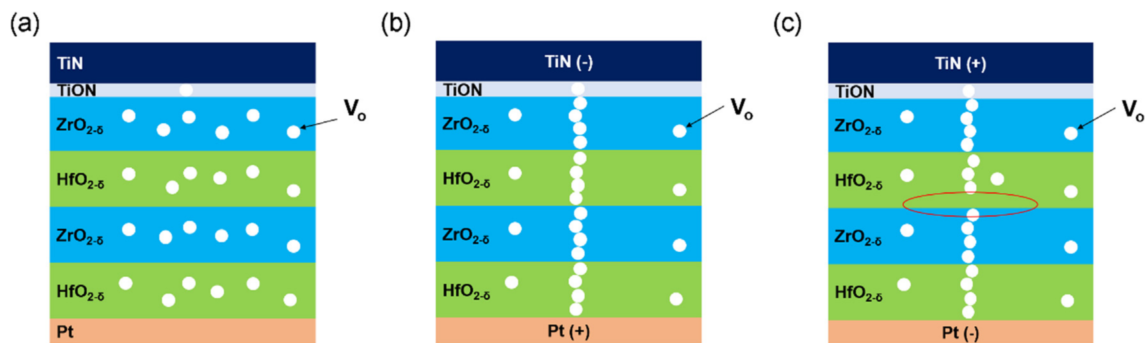

Fig. 9. Mechanism schematic diagrams of the N2 configuration on (a) initial state, (b) set process and (c) reset process.

owing to the decrease in transition barrier of oxygen vacancy in tetragonal/orthorhombic ZrO_2/HfO_2 and the increase in charged defects, leading to the dramatically fluctuation in R_{HRS}. Although additional work on the effects of the oxide/oxide interfaces and compliance current on the long-term endurance and retention is needed, these results illustrate the potential of HfO_2/ZrO_2 and relate nanolayer structures for investigating the fundamental characteristics and performance tuning of resistive switching devices.

CRediT authorship contribution statement

Lin Tang: Conceptualization, Writing - original draft. **Hiraku Maruyama:** Software, Writing - review & editing. **Taihao Han:** Validation, Investigation. **Juan C. Nino:** Resources, Writing - review & editing, Supervision. **Yonghong Chen:** Investigation. **Dou Zhang:** Resources, Supervision.

Declaration of Competing Interest

The authors declare that they have no known competing financial interests or personal relationships that could have appeared to influence the work reported in this paper.

Acknowledgements

The authors would like to acknowledge the financial support from State Key Laboratory of Powder Metallurgy and the National Natural Science Foundation of China (Grant Nos. U19A2087; 51672311). HM and JCN acknowledge the support of the US National Science Foundation under ECCS Award Number 1709641.

References

[1] M.H. Park, Y.H. Lee, H.J. Kim, Y.J. Kim, T. Moon, K.D. Kim, J. Muller, A. Kersch, U. Schroeder, T. Mikolajick, C.S. Hwang, Ferroelectricity and antiferroelectricity of doped thin HfO_2-based films, Adv. Mater. 27 (2015) 1811–1831.

[2] S.J. Kim, J. Mohan, C.D. Young, L. Colombo, J. Kim, Ferroelectric TiN/$Hf_{0.5}Zr_{0.5}O_2$/TiN capacitors with low-voltage operation and high reliability for next-generation FRAM applications, IEEE Int. Memory Workshop (IMW), Kyoto (2018) 1–4.

[3] B.T. Lin, Y.W. Lu, J. Shieh, M.J. Chen, Induction of ferroelectricity in nanoscale ZrO_2 thin films on Pt electrode without post-annealing, J. Eur. Ceram. Soc. 37 (2017) 1135–1139.

[4] T.S. Böscke, J. Müller, D. Bräuhaus, U. Schröder, U. Böttger, Ferroelectricity in hafnium oxide: CMOS compatible ferroelectric field effect transistors, 2011 International Electron Devices Meeting, IEEE, 2011, pp. 24–25.

[5] F. Ambriz-Vargas, G. Kolhatkar, M. Broyer, A. Hadj-Youssef, R. Nouar, A. Sarkissian, R. Thomas, C. Gomez-Yanez, M.A. Gauthier, A. Ruediger, A complementary metal oxide semiconductor process-compatible ferroelectric tunnel junction, ACS Appl. Mater. Inter. 9 (2017) 13262–13268.

[6] H. Luo, X. Zhou, C. Ellingford, Y. Zhang, S. Chen, K. Zhou, D. Zhang, C. Bowen, C. Wan, Interface design for high energy density polymer nanocomposites, Chem. Soc. Rev. 48 (2019) 4424–4465.

[7] H.Y. Yoong, H. Wu, J. Zhao, H. Wang, R. Guo, J. Xiao, B. Zhang, P. Yang, S.J. Pennycook, N. Deng, X. Yan, J. Chen, Epitaxial ferroelectric $Hf_{0.5}Zr_{0.5}O_2$ thin films and their implementations in memristors for brain-inspired computing, Adv. Funct. Mater. 28 (2018) 1–10.

[8] M. Lanza, A review on resistive switching in high-k dielectrics: A nanoscale point of view using conductive atomic force microscope, Mater. 7 (2014) 2155–2182.

[9] G.D. Wilk, R.M. Wallace, J.M. Anthony, High-k gate dielectrics, current status and materials properties considerations, J. Appl. Phys. 89 (2001) 5243–5275.

[10] B.L. Ellis, P. Knauth, T. Djenizian, Three-dimensional self-supported metal oxides for advanced energy storage, Adv. Mater. 26 (2014) 3368–3397.

[11] Y. Li, X. Li, L. Fu, R. Chen, H. Wang, X. Gao, Effect of interface layer engineering on resistive switching characteristics of ZrO_2-based resistive switching devices, IEEE T. Electron Dev. 65 (2018) 5390–5394.

[12] T.S. Böscke, J. Müller, D. Bräuhaus, U. Schröder, U. Böttger, Ferroelectricity in hafnium oxide thin films, Appl. Phys. Lett. 99 (2011) 102903.

[13] S.W. Ryu, S. Cho, J. Park, J. Kwac, H.J. Kim, Y. Nishi, Effects of ZrO_2 doping on HfO_2 resistive switching memory characteristics, Appl. Phys. Lett. 105 (2014) 072102.

[14] Z. Wu, J. Zhu, Enhanced unipolar resistive switching characteristics of $Hf_{0.5}Zr_{0.5}O_2$ thin films with high ON/OFF ratio, Mater. 10 (2017) 1–7.

[15] R. Waser, M. Aono, Nanoionics-based resistive switching memories, Nat. Mater. 6 (2007) 833–840.

[16] C.-Y. Huang, C.-Y. Huang, T.-L. Tsai, C.-A. Lin, T.-Y. Tseng, Switching mechanism of double forming process phenomenon in ZrO_x/HfO_y bilayer resistive switching memory structure with large endurance, Appl. Phys. Lett. 104 (2014).

[17] Y.C. Bae, A.R. Lee, J.B. Lee, J.H. Koo, K.C. Kwon, J.G. Park, H.S. Im, J.P. Hong, Oxygen ion drift-induced complementary resistive switching in homo $TiO_x/TiO_y/TiO_x$ and hetero TiO_x/TiON/TiO_x triple multilayer frameworks, Adv. Funct. Mater. 22 (2012) 709–716.

[18] J. Joshua Yang, F. Miao, M.D. Pickett, D.A. Ohlberg, D.R. Stewart, C.N. Lau, R.S. Williams, The mechanism of electroforming of metal oxide memristive switches, Nanotechnology 20 (2009) 215201.

[19] T.-J. Chu, T.-M. Tsai, T.-C. Chang, K.-C. Chang, C.-H. Pan, K.-H. Chen, J.-H. Chen, H.-L. Chen, H.-C. Huang, C.-C. Shih, Y.-E. Syu, J.-C. Zheng, S.M. Sze, Ultra-high resistive switching mechanism induced by oxygen ion accumulation on nitrogen-doped resistive random access memory, Appl. Phys. Lett. 105 (2014) 223514.

[20] G. Niu, M.A. Schubert, S.U. Sharath, P. Zaumseil, S. Vogel, C. Wenger, E. Hildebrandt, S. Bhupathi, E. Perez, L. Alff, M. Lehmann, T. Schroeder, T. Niermann, Electron holography on HfO_2/HfO_{2-x} bilayer structures with multilevel resistive switching properties, Nanotechnology 28 (2017) 215702.

[21] S.-Y. Wang, D.-Y. Lee, T.-Y. Tseng, C.-Y. Lin, Effects of Ti top electrode thickness on the resistive switching behaviors of rf-sputtered ZrO_2 memory films, Appl. Phys. Lett. 95 (11) (2009).

[22] H. Choi, J. Yi, S. Hwang, S. Lee, S. Song, S. Lee, J. Lee, D. Son, J. Park, S.-J. Kim, J.-Y. Kim, S. Lee, J. Moon, C. Kim, J. Park, M. Joo, J. Roh, S. Park, S.-W. Chung, J. Rhee, S.J. Hong, The effect of tunnel barrier at resistive switching device for low power memory applications, 2011 3rd IEEE International Memory Workshop (IMW), IEEE, 2011, pp. 1–4.

[23] J.-K. Lee, S. Jung, J. Park, S.-W. Chung, J.S. Roh, S.-J. Hong, I.H. Cho, H.-I. Kwon, C.H. Park, B.G. Park, J.-H. Lee, Accurate analysis of conduction and resistive-switching mechanisms in double-layered resistive-switching memory devices, Appl. Phys. Lett. 101 (2012) 103506.

[24] A. Sawa, Resistive switching in transition metal oxides, Mater. Today 11 (2008) 28–36.

[25] A.S. Foster, F. Lopez Gejo, A.L. Shluger, R.M. Nieminen, Vacancy and interstitial defects in hafnia, Phys. Rev. B 65 (2002) 174117.

[26] C. Tang, B. Tuttle, R. Ramprasad, Diffusion of O vacancies near Si:HfO_2 interfaces: An ab initio investigation, Phys. Rev. B 76 (2007) 073306.

[27] M. Shandalov, P.C. Mclntyre, Size-dependent polymorphism in HfO_2 nanotubes and nanoscale thin films, J. Appl. Phys. 106 (2009) 084322.

[28] A. Navrotsky, Thermochemical insights into refractory ceramic materials based on oxides with large tetravalent cations, J. Mater. Chem. 15 (2005) 1883–1890.

[29] S. Yu, X. Guan, H.S.P. Wong, Conduction mechanism of TiN/HfO_x/Pt resistive switching memory: A trap-assisted-tunneling model, Appl. Phys. Lett. 99 (2011) 063507.

[30] D.D. Sarma, C.N.R. Rao, XPES studies of oxides of second- and third-row transition metals including rare earths, J. Electron Spectrosc. 20 (1980) 25–45.

[31] M. Qi, Y. Tao, Z. Wang, H. Xu, X. Zhao, W. Liu, J. Ma, Y. Liu, Highly uniform switching of HfO_{2-x} based RRAM achieved through Ar plasma treatment for low power and multilevel storage, Appl. Surf. Sci. 458 (2018) 216–221.